



## Full Length Article

## The effect of grain boundary on irradiation resistance of CoCrCuFeNi high entropy alloy

Rui Li<sup>a,\*</sup>, Yidong Li<sup>a</sup>, Yu Liu<sup>a</sup>, Qing Peng<sup>b,c,d,\*</sup><sup>a</sup> School of Mechanical Engineering, University of Science and Technology Beijing, Beijing, 100083, China<sup>b</sup> Physics Department, King Fahd University of Petroleum & Minerals, Dhahran 31261, Saudi Arabia<sup>c</sup> K.A.CARE Energy Research & Innovation Center at Dhahran, Dhahran, 31261, Saudi Arabia<sup>d</sup> Interdisciplinary Research Center for Hydrogen and Energy Storage, King Fahd University of Petroleum and Minerals, Dhahran 31261, Saudi Arabia

## ARTICLE INFO

## ABSTRACT

## Keywords:

High entropy alloy  
Grain boundaries  
Irradiation resistance  
Defects

Defect traps have been well known to influence the irradiation resistance of traditional structural materials, but to what extent is not fully clear for high entropy alloys. Herein, the effect of grain boundary on irradiation resistance of CoCrCuFeNi is investigated through defects capture, strength variation, and void annihilation via molecular dynamics simulations and compared to that of pure Ni, taking  $\Sigma 5(210)$  as a representative grain boundary. The grain boundaries in both CoCrCuFeNi and Ni are effective in capturing point defects. The number of captured defects is related to the distance between primary knock-on atoms and grain boundary. The change in tensile stress of CoCrCuFeNi after irradiation is smaller than that of Ni. The grain boundary of CoCrCuFeNi can annihilate voids at room temperature. However, that of Ni is hindered in the migration process and cannot annihilate voids completely. Our results provide atomistic insights into the mechanism of radiation resistance via grain boundaries as recombination centers.

## 1. Introduction

Green energy is highly desirable for sustainable development of modern society and the future of civilization. As one of the major kinds of green energy, nuclear energy has attracted extensive attention [1]. With the development of the generation IV nuclear reactors, nuclear structural materials are supplied to work under severe conditions such as high temperature, strong corrosion, long time (years or decades) and high-dose neutron irradiation [2]. These extreme work conditions call for high radiation tolerant structural materials. High entropy alloys (HEAs) are one of the good candidates for radiation tolerant materials. Yeh *et al.* [3] and Cantor *et al.* [4] proposed HEAs in 2004, which are multi-element alloys that are composed of five or more elements. High configuration entropy prevents the formation of intermetallic compounds, and promotes the formation of single-phase FCC or BCC structures. Meanwhile, the combination of various elements results in serious lattice distortion [5,6] and slow diffusion effect [7–9]. HEAs represent a new strategy for designing materials with mechanical properties superior to those of conventional alloys, such as high hardness [10], excellent low-temperature fracture toughness [11], and high strength [12].

It has been reported that HEAs have excellent radiation resistance. Lu

*et al.* [13] investigated the He ions irradiation resistance of  $Ti_2ZrHfV_{0.5}Mo_{0.2}$ . They found that the hardness of the HEA was almost the same before and after irradiation. The density of the helium bubbles in the sample was far lower than the experimental value of traditional alloy. Xia *et al.* [14] studied the irradiation resistance of  $Al_xCoCrFeNi$  ( $x = 0.1, 0.75, 1.5$ ) under 3 MeV Au ions. No phase decomposition was observed after irradiation owing to the high configuration entropy, high defect formation energy and migration energy, and low thermal conductivity. Some works suggested that nanocrystalline HEAs performed better in irradiation resistance owing to more grain boundaries. Nagase *et al.* [15] observed nanocrystalline CoCrCuFeNi under electron irradiation by in-situ transmission electron microscopy (TEM). Their results showed that the sample still maintained high phase stability, and the grain size did not increase even if the irradiation dose reached 40 dpa. Meanwhile, Zhang *et al.* [16] used 3 MeV Ni ions to irradiate nanocrystalline CoCrCuFeNi HEA. When the irradiation dose reached 600 dpa, the FCC phase remained stable. El-Atwani *et al.* [17] indicated that no dislocation loops were observed in  $WTaCrV$  refractory HEA even when the 1 MeV  $Kr^{2+}$  irradiation dose reached 8 dpa, and nano-indentation showed that there was almost no irradiation hardening. Pu *et al.* [18] prepared ultrafine nanocrystalline  $Al_{1.5}CoCrFeNi$  with single-

\* Corresponding authors.

E-mail addresses: [lirui@ustb.edu.cn](mailto:lirui@ustb.edu.cn) (R. Li), [qing.peng@kfupm.edu.sa](mailto:qing.peng@kfupm.edu.sa) (Q. Peng).

phase structure and irradiated it with 60 keV He to a flux of  $1 \times 10^{17} \text{ cm}^{-2}$ . Due to the defect absorption effect of nano grain boundaries, helium clusters will distribute along the grain boundaries.

Molecular dynamics simulations have been successfully applied to investigate displacement cascade damage [19–21]. However, the study on the interaction of grain boundary and displacement cascade interaction only aims at the alloys that are composed of 4 elements or less in the literature. Cusentino *et al.* [22] investigated the interaction between  $\Sigma 5$  tilted grain boundaries and cascade in FeCoCrNi and Ni under different primary knock-on atom (PKA) energies. They concluded that the number of residual point defects in HEA was less than that in Ni after the reaction of ordered and disordered grain boundaries with cascade. Pérez-Pérez *et al.* [23] investigated the behavior of radiation damage on symmetrically tilted and twisted grain boundary structures in BCC iron. They found that the interstitial clusters were more extensively induced near the twisted boundary than the tilted boundary. Zhang *et al.* [24] studied the interaction between different types of grain boundaries and cascade in W. The results showed that the distance between PKA and grain boundary was very important to the formation of defects. Tschopp *et al.* [25] investigated the energetics and length scales associated with the interaction between point defects and the grain boundaries in BCC iron. Their results revealed the influence of local atomic structure and grain boundary character on the point defect formation energy. Kedharnath *et al.* [26] studied the effect of different kinds of grain boundaries in  $\alpha$ -Fe, and found that the formation energy of defects inside the grain boundary was much lower than that outside. They also found that the low-angle grain boundary had a higher capture efficiency for defects.

Despite the aforementioned efforts, a full understanding of the effect of grain boundary on the displacement cascade in five-element HEAs is still lacking. Therefore, in this study, we aim to investigate the interaction between grain boundary and cascade in CoCrCuFeNi HEA with reference to single-element Ni metal. The method of molecular dynamics simulations is suitable and is applied in the investigation. The results show that the capture of point defects by grain boundary is effective. The number of captured point defects is positively correlated with the separation of PKA and grain boundary. In addition, the absorption of void by grain boundary in the two materials is compared and analyzed.

## 2. Model and method

We take the  $\sum 5(210)$  grain boundary as the representative grain boundary in FCC crystals [27] throughout this work. As a typical large angle grain boundary, the atomistic configuration of a  $\sum 5(210)$  grain boundary is created in our CoCrCuFeNi and Ni models, as shown in Fig. 1. The size of the model is  $10\sqrt{5}a_0 \times 22\sqrt{5}a_0 \times 22a_0$ , the lattice constant  $a_0$  of CoCrCuFeNi is 0.3552 nm [28], and the lattice constant  $a_0$  of pure Ni is 0.352 nm [29]. The numbers of atoms in the two materials are both 96800. The X, Y and Z directions are along the [100], [010]

and [001] crystal orientations, respectively. The grain boundary is perpendicular to Y axis. To prevent the movement of models in the cascade process, the three-layer atoms at the top and bottom in Y direction are fixed [30]. Non-periodic boundary condition is applied along Y direction. Periodic boundary conditions are applied along X and Z directions.

To investigate the effect of separation between PKA and grain boundary on defect creation, atoms from -1 to 5 nm away from grain boundary are selected as PKAs. The energy of initial PKA atoms is 5 keV consistent with the size of the model [31]. The initial velocity is along -Y direction. The simulated temperature is 300 K during NVT stage [32]. The large-scale parallel computing software LAMMPS is used to simulate the whole cascade process [33]. The five element potential that was fitted by Deluigi *et al.* [34] is applied to describe the interactions of atoms in CoCrCuFeNi HEA. The single element potential fitted by Stoller *et al.* [35] is applied to describe the interaction among atoms in Ni. Both potentials include the ZBL potential [36], which is widely used in interatomic potentials applicable for radiation damage simulation. The ZBL potential can accurately describe the repulsive interactions at short interatomic distances.

The simulation procedure is as follows. First the conjugate gradient method is applied to minimize the potential energy of the model. Then the systems are relaxed for 60 ps under canonical ensemble (NVT), which makes the system reach equilibrium. The microcanonical ensemble (NVE) is applied after the cascade process starts. The time step is 0.001 ps. To model the heat dissipation beyond the boundary of the simulation boxes, a thermostat region of 0.5 nm thickness is set in the outermost layer of the boxes. Berendsen thermostat is applied to control the pressure and temperature, respectively, of the system [37]. To simulate fast collision process, an adaptive variable step is used to ensure that atomic moving distance is less than 0.002 nm in every single step. The whole cascade process lasts for 100 ps. Three simulation processes are carried out at each position of PKAs from the grain boundary to reduce the statistic error. The initial PKA atom for each simulation is chosen randomly and the distance to the grain boundary is constant. OVITO is applied to analyze the defects during the whole cascade process [38].

Wigner-Seitz defect analysis is used to identify point defects generated by the displacement cascades. The point defects here are divided into two categories, as shown in Fig. 2. The interstitials and vacancies remaining outside the grain boundary region are represented by Ir and Vr, respectively. The other interstitials and vacancies absorbed by the grain boundary are represented by Ia and Va.

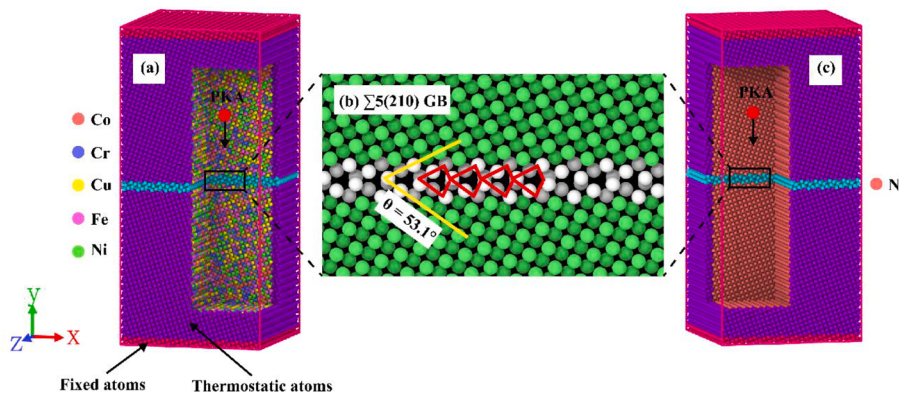


**Fig. 1.** The model of grain boundary in CoCrCuFeNi and Ni. (a) CoCrCuFeNi. (b) The grain boundary. Green sphere represents FCC structure, and white sphere represents unrecognized structure. (c) Ni. (For interpretation of the references to color in this figure legend, the reader is referred to the web version of this article.)

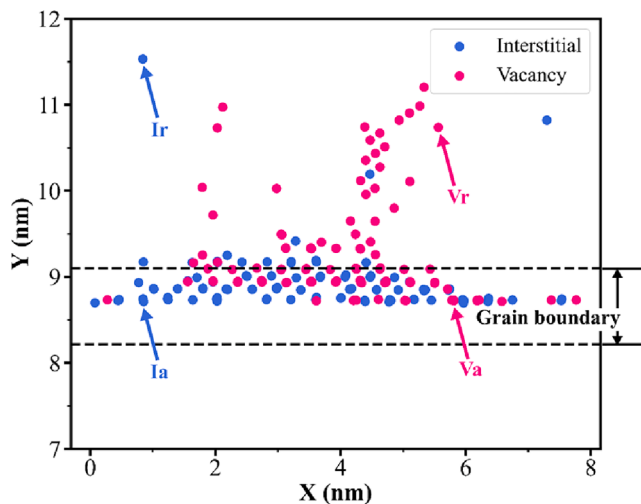


Fig. 2. The illustration of distribution of point defects after cascade.

### 3. Results and discussion

#### 3.1. Formation and evolution of point defects

The layer-wise average atomic potential energy [39] of the model is calculated, as shown in Fig. 3(a), where '0' of the abscissa represents the center of the grain boundary. The atomic potential energy inside the grain boundary region is much higher than that outside the grain boundary region because the atomic arrangement inside the grain boundary is irregular. The atomic configuration near grain boundary is shown in Fig. 3(b). The layer-wise average potential energy outside the grain boundary region in CoCrCuFeNi shows fluctuations with respect to the layer position owing to the complexity of elements. Since Ni only contains one element, the standard deviation of the average potential energy outside the grain boundary region is almost zero. The average potential energy in CoCrCuFeNi and Ni is symmetrical along the grain boundary center. The range of higher potential energy is the width of grain boundary, as shown in Fig. 3. The grain boundaries of the materials are both  $\sum 5(210)$ . The widths of the grain boundaries in CoCrCuFeNi and Ni are 0.81 nm and 0.89 nm, respectively, which are similar.

The cascade simulations are carried out at seven positions where PKA is  $-1 \sim 5$  nm from grain boundary. The interstitials and vacancies captured by grain boundary are represented by ab\_SIAs and ab\_Vacs, respectively. The residual interstitials and vacancies outside the grain boundary region are represented by re\_SIAs and re\_Vacs, respectively. As shown in Fig. 4(a), at first, the absorption of defects by grain boundary

in CoCrCuFeNi and Ni increases and then decreases, which indicates that the ability of grain boundary to capture defects is related to the distance between PKA and grain boundary. Grain boundaries prefer to capture interstitials. When the distance between PKA and grain boundary is 1 ~ 2 nm, more than 80 % of total interstitials and vacancies produced by cascades in the two materials are absorbed by grain boundary. The absorption of both interstitials and vacancies help to increase the probability of point defect annihilation. Although more defects are absorbed by grain boundary in Ni than in CoCrCuFeNi, the number of residual point defects in Ni is larger, as shown in Fig. 4(b), which implies more defects in Ni. Consequently, more defects in Ni lead to more defects being absorbed by grain boundary. However, the difference between the proportion of the absorption rate  $\frac{\text{ab\_SIAs}}{\text{re\_SIAs+ab\_SIAs}}$  is only approximately 2.75 %, which is negligible. When the distance between the PKA and grain boundary is  $-1 \sim 2$  nm, the number of point defects remaining outside the grain boundary in CoCrCuFeNi decreases, whereas it increases at first and then decreases in Ni, as shown in Fig. 4(b). Moreover, the residual point defects in CoCrCuFeNi and Ni are the least at 2 nm.

When the distance between PKA and grain boundary is  $2 \sim 5$  nm, the number of residual point defects outside grain boundary in CoCrCuFeNi slightly increases due to the weakened interaction between PKA and grain boundary. We define the critical distance as the distance where grain boundary is far from the center of PKA but still absorbs interstitials [24]. The critical distance in CoCrCuFeNi high entropy alloy is 2 nm, as shown in Fig. 4(a). The critical distance in Ni is close to 3 nm. At this distance, the opportunity for the recombination of interstitials and vacancies outside the grain boundary region decreases. Then the largest number of vacancies remain outside grain boundary. When the distance between PKA and grain boundary is  $4 \sim 5$  nm, the number of point defects remaining outside grain boundary in Ni decreases. The reason is that the distance between PKA and grain boundary is large, which results in a low total number of point defects. It is worth noting that our results from the  $\sum 5(210)$  grain boundary configuration could be generalized to other grain boundaries since the underlying trapping mechanism is the same [27].

To further uncover the effect of grain boundary on the irradiation resistance of CoCrCuFeNi and Ni, we have analyzed the evolution of point defects at 2 nm. The distance of 2 nm is selected because the interaction between the grain boundary and cascade reaches a maximum. The number of point defects remaining outside the grain boundary region in CoCrCuFeNi and Ni is relatively small. The same scale is applied to compare the spatial distribution of point defects. The number of point defects in CoCrCuFeNi reaches a maximum at 0.32 ps, as shown in Fig. 5. The distribution is more dispersed. The point defects in Ni reach a maximum at 0.36 ps, but the distribution is similar to a sphere. Following the evolution process, the average distance between

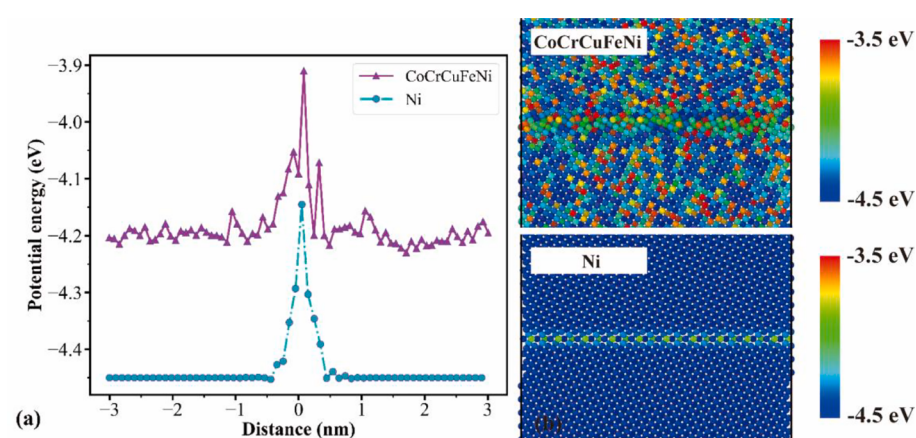
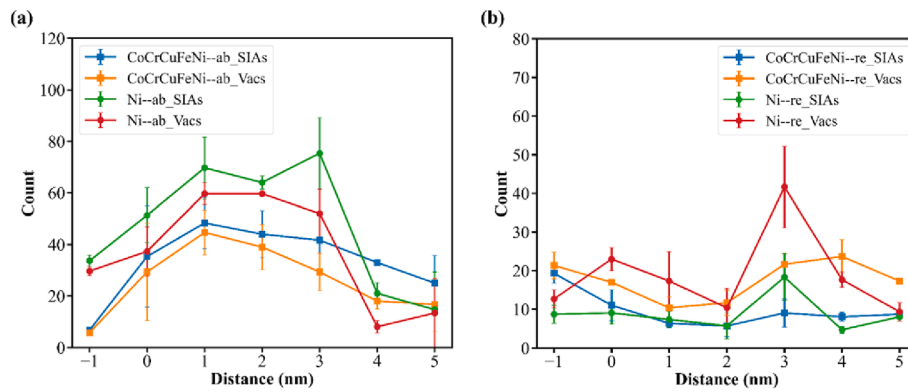
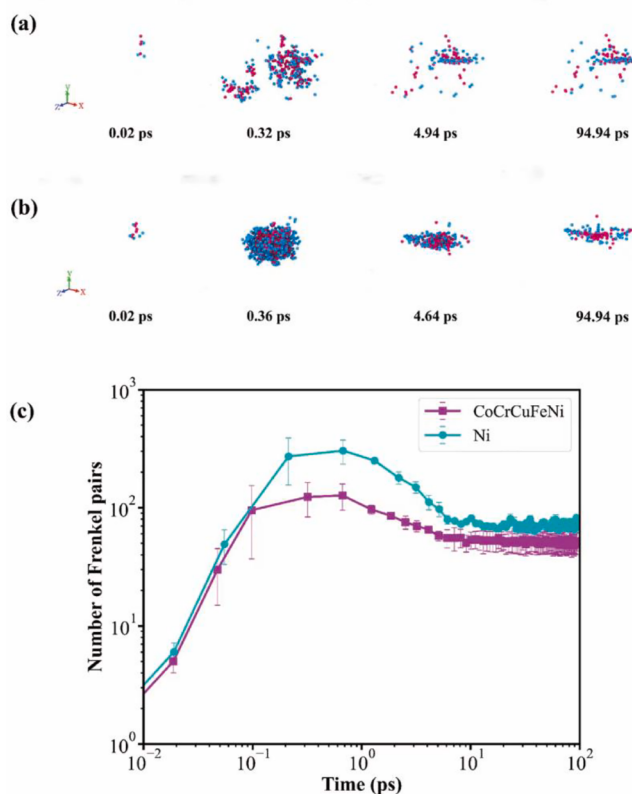


Fig. 3. (a) Average potential energy of each layer of atoms in CoCrCuFeNi and Ni along Y direction. (b) Atomic configuration near grain boundary. The color represents the level of potential energy.



**Fig. 4.** The point defects after the cascade process. (a) The interstitials and vacancies of CoCrCuFeNi and Ni captured by grain boundary are represented by ab\_SIAs and ab\_Vacs, respectively. (b) The residual interstitials and vacancies of CoCrCuFeNi and Ni outside the grain boundary region are represented by re\_SIAs and re\_Vacs, respectively.



**Fig. 5.** The evolution of point defects in CoCrCuFeNi and Ni at a distance of 2 nm between PKA and grain boundary. (a) CoCrCuFeNi. (b) Ni. (c) Total point defects (re\_SIAs + ab\_SIAs) generated during the cascade process.

the point defects in CoCrCuFeNi and the center of grain boundary in Y direction is 0.53 nm at 94.94 ps. However, the average distance between the point defects in Ni and the grain boundary center in Y direction is only 0.01 nm. The result is consistent with the number of point defects absorbed by grain boundary in Fig. 4(a), which shows that more absorbed defects occur in Ni than in CoCrCuFeNi. Nevertheless, it is found from Fig. 5(c) that the total number of point defects generated by CoCrCuFeNi irradiation is less than that of Ni, resulting in the same number of point defects remaining outside the grain boundary.

### 3.2. The tensile stress before and after irradiation

When the materials undergo irradiation, the microstructure changes.

As a result, the mechanical properties change accordingly. To what extent, however, is desirable but unknown. Therefore, it is necessary to analyze the change in mechanical properties of CoCrCuFeNi with grain boundary after irradiation. Here, we calculate the tensile stress of CoCrCuFeNi before and after irradiation and compare it to that of Ni by simulating the tensile process of those two materials.

As shown in Fig. 6(a), the upper and lower layers with a thickness of 1 nm are rigid body. The lower rigid body is fixed. A tensile speed of 40 m/s is applied on the upper rigid layers along the Y direction. The simulation temperature is 300 K. Here the models after irradiation are those in which PKA is 2 nm away from the grain boundary. The tensile stress-strain curves of CoCrCuFeNi and Ni are shown in Fig. 6(b). The maximum point of the curve is defined as the ultimate tensile stress, and the corresponding strain is the ultimate tensile strain [39]. The curve drops rapidly after the ultimate tensile stress, which indicates the fracture failure of the material.

Note that our models are ideal crystals without any imperfections, which means that the dislocations are absent. It differs from a real crystal where dislocations are inevitable. Therefore, the ultimate tensile stress is expected to be much larger in our models. For example, Sun *et al.* [40] calculated that the tensile strength of CoCrFeNi(Al<sub>0.3</sub>Ti<sub>0.2</sub>)<sub>0.5</sub> via molecular dynamics was 19.1 GPa. However, the experimental result was only 1132.6 MPa. The simulation results of our model are summarized in Table 1. The vacancy caused by irradiation makes the material easier to crack during the tensile process and lowers its mechanical properties [39]. Therefore, the ultimate tensile stress of CoCrCuFeNi HEA and Ni after irradiation decreases to some extent. The change ( $= \frac{\text{Unirradiated} - \text{Irradiated}}{\text{Unirradiated}} * 100\%$ ) of CoCrCuFeNi is only 0.40 %, while that of Ni is 10.25 %. Although the grain boundary in Ni absorbs more point defects, the total point defects in the cascade of CoCrCuFeNi HEA are fewer. As a result, the change in the tensile stress of CoCrCuFeNi after irradiation is lower. Meanwhile, the tensile strain loss of CoCrCuFeNi after irradiation is only 1.12 %, which is much lower than the 17.09 % loss of Ni, indicating less ductility loss of CoCrCuFeNi after irradiation. The results show that CoCrCuFeNi performs better in radiation resistance.

### 3.3. Interaction between grain boundary and void

The point defects generated by the cascade may form larger size defects after long-term diffusion and migration, such as voids, stacking fault tetrahedrons, precipitates and bubbles. These defects have a significant impact on the mechanical properties of materials, especially the voids formed by vacancy aggregation. In turn, they cause the swelling of materials. Therefore, it is necessary to study the interaction between grain boundary and void. Zhang *et al.* [41] investigated the interaction between voids and GBs by molecular dynamics simulations and

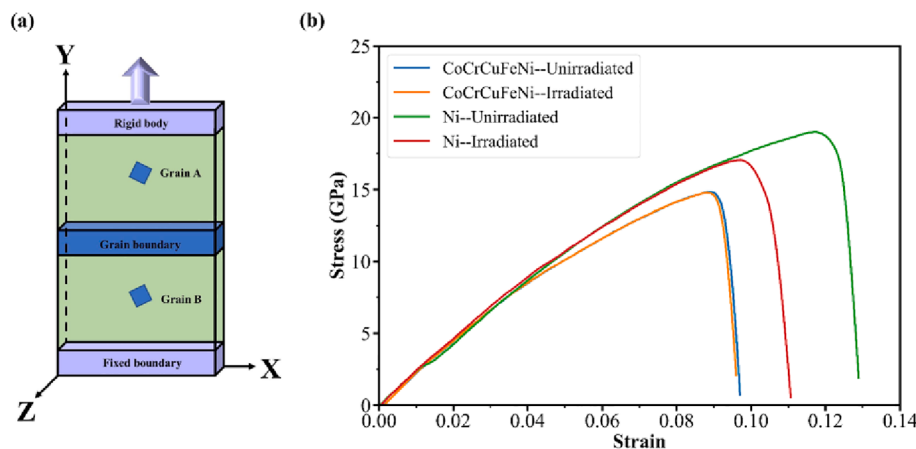


**Fig. 6.** Tensile simulation of CoCrCuFeNi and Ni. (a) The illustration of tensile model with grain boundary in materials. (b) Tensile stress–strain curve of CoCrCuFeNi and Ni before and after irradiation.

**Table 1**

The tensile stress and tensile strain before and after irradiation.

	Ultimate tensile stress (GPa)			Ultimate tensile strain		
	Unirradiated	Irradiated	Loss (%)	Unirradiated	Irradiated	Loss (%)
CoCrCuFeNi	14.84	14.78	0.40	0.089	0.088	1.12
Ni	19.02	17.07	10.25	0.117	0.097	17.09

examined the effect of void size on the interaction. Referring to Zhang *et al.*'s study, a void diameter value of 1.8 nm is suitable to investigate the interaction between grain boundary and void. A  $\sum 5(210)$  large angle grain boundary and a void with a diameter of 1.8 nm are posited at 1/5 and 5/12 of Y direction of the model, respectively. The initial distance between them is approximately 3.6 nm to ensure that the interaction between grain boundary and void is negligible before the shear process. The thickness of 0.5 nm is set as rigid at the upper and lower ends of the model, and the upper rigid body is fixed. The temperature is 300 K, and the simulation system relaxes for 20 ps under NVT ensemble to achieve thermodynamic equilibrium. A shear velocity of 30 m/s is applied to the lower rigid layers along X direction, and the grain boundary will move along Y direction driven by the shear stress [42].

The interaction between grain boundary and void in CoCrCuFeNi and Ni is shown in Fig. 7. The shear process has not started at times I and IV. The distance between grain boundary and void is large. Following the shear process, the grain boundary continues to migrate upward until it encounters void to hinder its migration. Then, Shockley dislocation nucleation occurs during the interaction between void and grain boundary in CoCrCuFeNi, as shown at time II. Zhang *et al.* pointed out that the nucleation and propagation of dislocations near the void could promote the reduction in void size and even annihilation during the interaction between grain boundary and void in Cu [41]. Our results of

CoCrCuFeNi HEA are consistent with those of single element Cu.

When the shear deformation continues to increase, as shown at time III, the void in CoCrCuFeNi is annihilated by the grain boundary, leaving only some small defect clusters. The void in Ni also interacts with the grain boundary at time V to form dislocation nucleation. However, the formed dislocations also have stair-rod dislocations in addition to Shockley dislocations. The newly formed stair-rod dislocation evolves into partial stacking fault tetrahedron. While grain boundary can provide a significant energetic driving force for the aggregation of interstitial atoms, the radiation-induced vacancies and their clusters typically exhibit lower mobility than the interstitial atoms [43]. Stacking fault tetrahedron is a vacancy-type defect in FCC metals during irradiation, which seriously hinders the migration of grain boundary. Moreover, multiple peaks of shear stress are higher than those of CoCrCuFeNi. The void is still not annihilated in Ni at time VI. The reason for the difference between CoCrCuFeNi and Ni is that the atomic-level heterogeneity in high entropy alloys results in sluggish diffusion, which makes the interstitial atoms migrate slower, and thus suppresses the transformation of void to stacking fault tetrahedron [44]. Therefore, it does not affect the annihilation of void by grain boundary. The above results show that CoCrCuFeNi has better irradiation resistance.

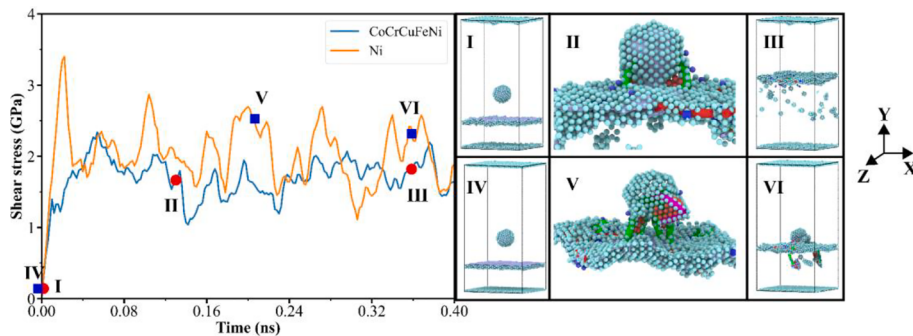


**Fig. 7.** The shear stress and the interaction process between  $\sum 5(210)$  grain boundary and void in CoCrCuFeNi and Ni. Light blue, light red, blue atoms represent unrecognized structure, HCP and BCC structure. Green, blue, purple, and red lines at II and V represent 1/6  $\langle 112 \rangle$  Shockley dislocation, 1/2  $\langle 110 \rangle$  Perfect dislocation, 1/6  $\langle 110 \rangle$  Stair-rod dislocation, and unrecognized dislocation, respectively. (For interpretation of the references to color in this figure legend, the reader is referred to the web version of this article.)

#### 4. Conclusions

The influence of grain boundary on the irradiation resistance of CoCrCuFeNi HEA and pure Ni single crystal has been investigated by molecular dynamics simulations. The results show that the grain boundary can effectively absorb point defects. The number of absorbed point defects depends on the separation between PKA and grain boundary. The grain boundary tends to absorb more interstitials than vacancies. The critical distance between PKA and grain boundary is 2 nm, where their interaction is non-trivial. Beyond this distance, the number of residual point defects outside the grain boundary region in CoCrCuFeNi and Ni are negligible.

The tensile stress of CoCrCuFeNi shows less reduction after irradiation than that of Ni, which implies better irradiation resistance. The interaction between grain boundary and void shows that the grain boundary of CoCrCuFeNi can annihilate the void, but the void in Ni will evolve into partial stacking fault tetrahedron, which hinders the annihilation of void by grain boundary. Our atomistic insights into the influence of grain boundary as a defect trap on irradiation resistance in high entropy alloys indicate that high entropy alloys are promising anti-irradiation materials.

#### CRediT authorship contribution statement

**Rui Li:** Conceptualization, Formal analysis, Funding acquisition, Investigation, Methodology, Project administration, Resources, Supervision, Writing – original draft, Writing – review & editing. **Yidong Li:** Data curation, Formal analysis, Methodology, Validation, Writing – original draft, Writing – review & editing. **Yu Liu:** Investigation, Methodology, Software, Visualization, Writing – original draft. **Qing Peng:** Funding acquisition, Project administration, Resources, Writing – review & editing.

#### Declaration of Competing Interest

The authors declare that they have no known competing financial interests or personal relationships that could have appeared to influence the work reported in this paper.

#### Data availability

Data will be made available on request.

#### Acknowledgement

The work is supported by the Fundamental Research Funds for the Central Universities (No. FRF-IDRY-20-008). Q.P. would like to acknowledge the support provided by the Deanship of Scientific Research (DSR) at King Fahd University of Petroleum & Minerals (KFUPM) for funding this work through project No. DF201020.

#### Data Availability Statement

Data available on request from the authors.

#### References

- [1] R.B. Duffey, Sustainable futures using nuclear energy, *Prog. Nucl. Energy* 47 (1–4) (2005) 535–543.
- [2] S.J. Zinkle, G. Was, Materials challenges in nuclear energy, *Acta Mater.* 61 (3) (2013) 735–758.
- [3] J.W. Yeh, S.K. Chen, S.J. Lin, J.Y. Gan, T.S. Chin, T.T. Shun, C.H. Tsau, S.Y. Chang, Nanostructured high-entropy alloys with multiple principal elements: novel alloy design concepts and outcomes, *Adv. Eng. Mater.* 6 (5) (2004) 299–303.
- [4] B. Cantor, I. Chang, P. Knight, A. Vincent, Microstructural development in equiaxed multicomponent alloys, *Mater. Sci. Eng. A* 375 (2004) 213–218.
- [5] D.B. Miracle, O.N. Senkov, A critical review of high entropy alloys and related concepts, *Acta Mater.* 122 (2017) 448–511.
- [6] Z. Wang, Q. Fang, J. Li, B. Liu, Y. Liu, Effect of lattice distortion on solid solution strengthening of BCC high-entropy alloys, *J. Mater. Sci. Technol.* 34 (2) (2018) 349–354.
- [7] K.-Y. Tsai, M.-H. Tsai, J.-W. Yeh, Sluggish diffusion in Co–Cr–Fe–Mn–Ni high-entropy alloys, *Acta Mater.* 61 (13) (2013) 4887–4897.
- [8] J.-W. Yeh, Physical metallurgy of high-entropy alloys, *JOM* 67 (10) (2015) 2254–2261.
- [9] M. Vaidya, S. Trubel, B. Murty, G. Wilde, S.V. Divinski, Ni tracer diffusion in CoCrFeNi and CoCrFeMnNi high entropy alloys, *J. Alloy. Compd.* 688 (2016) 994–1001.
- [10] P.K. Huang, J.W. Yeh, T.T. Shun, S.K. Chen, Multi-principal-element alloys with improved oxidation and wear resistance for thermal spray coating, *Adv. Eng. Mater.* 6 (1–2) (2004) 74–78.
- [11] B. Gludovatz, A. Hohenwarter, K.V. Thurston, H. Bei, Z. Wu, E.P. George, R. O. Ritchie, Exceptional damage-tolerance of a medium-entropy alloy CrCoNi at cryogenic temperatures, *Nat. Commun.* 7 (1) (2016) 1–8.
- [12] F. Otto, A. Dlouhý, C. Somsen, H. Bei, G. Eggeler, E.P. George, The influences of temperature and microstructure on the tensile properties of a CoCrFeMnNi high-entropy alloy, *Acta Mater.* 61 (15) (2013) 5743–5755.
- [13] Y. Lu, H. Huang, X. Gao, C. Ren, J. Gao, H. Zhang, S. Zheng, Q. Jin, Y. Zhao, C. Lu, A promising new class of irradiation tolerant materials: Ti2ZrHfV0.5Mo0.2 high-entropy alloy, *J. Mater. Sci. Technol.* 35 (3) (2019) 369–373.
- [14] S. Xia, M.C. Gao, T. Yang, P.K. Liaw, Y. Zhang, Phase stability and microstructures of high entropy alloys ion irradiated to high doses, *J. Nucl. Mater.* 480 (2016) 100–108.
- [15] T. Nagase, P.D. Rack, J.H. Noh, T. Egami, In-situ TEM observation of structural changes in nano-crystalline CoCrCuFeNi multicomponent high-entropy alloy (HEA) under fast electron irradiation by high voltage electron microscopy (HVEM), *Intermetallics* 59 (2015) 32–42.
- [16] Y. Zhang, M.A. Tunéz, M.L. Crespillo, F. Zhang, W.L. Boldman, P.D. Rack, L. Jiang, C. Xu, G. Greaves, S.E. Donnelly, Thermal stability and irradiation response of nanocrystalline CoCrCuFeNi high-entropy alloy, *Nanotechnology* 30 (29) (2019), 294004.
- [17] O. El-Atwani, N. Li, M. Li, A. Devaraj, J. Baldwin, M.M. Schneider, D. Sobieraj, J. S. Wróbel, D. Nguyen-Manh, S.A. Maloy, Outstanding radiation resistance of tungsten-based high-entropy alloys, *Sci. Adv.* 5 (3) (2019) eaav2002.
- [18] G. Pu, L. Lin, R. Ang, K. Zhang, B. Liu, B. Liu, T. Peng, S. Liu, Q. Li, Outstanding radiation tolerance and mechanical behavior in ultra-fine nanocrystalline Al1.5CoCrFeNi high entropy alloy films under He ion irradiation, *Appl. Surf. Sci.* 516 (2020), 146129.
- [19] H.-S. Do, B.-J. Lee, Origin of radiation resistance in multi-principal element alloys, *Sci. Rep.* 8 (1) (2018) 1–9.
- [20] Q. Peng, F. Meng, Y. Yang, C. Lu, H. Deng, L. Wang, S. De, F. Gao, Shockwave generates  $< 100 >$  dislocation loops in bcc iron, *Nat. Commun.* 9 (1) (2018) 1–6.
- [21] Y. Lin, T. Yang, L. Lang, C. Shan, H. Deng, W. Hu, F. Gao, Enhanced radiation tolerance of the Ni–Co–Cr–Fe high-entropy alloy as revealed from primary damage, *Acta Mater.* 196 (2020) 133–143.
- [22] M. Cusentino, M. Wood, R. Dingreville, Compositional and structural origins of radiation damage mitigation in high-entropy alloys, *J. Appl. Phys.* 128 (12) (2020), 125904.
- [23] F.J. Pérez-Pérez, R. Smith, Structural changes at grain boundaries in bcc iron induced by atomic collisions, *Nucl. Instrum. Methods Phys. Res., Sect. B* 164–165 (2000) 487–494.
- [24] C. Zhang, W. Zhou, Y. Li, Z. Zeng, X. Ju, Primary radiation damage near grain boundary in bcc tungsten by molecular dynamics simulations, *J. Nucl. Mater.* 458 (2015) 138–145.
- [25] M.A. Tschopp, K.N. Solanki, F. Gao, X. Sun, M.A. Khaleel, M.F. Horstemeyer, Probing grain boundary sink strength at the nanoscale: energetics and length scales of vacancy and interstitial absorption by grain boundaries in  $\alpha$ -Fe, *Phys. Rev. B* 85 (6) (2012), 064108.
- [26] A. Kedarnath, R. Kapoor, A. Sarkar, Atomistic simulation of interaction of collision cascade with different types of grain boundaries in  $\alpha$ -Fe, *J. Nucl. Mater.* 523 (2019) 444–457.
- [27] L. Zhang, C. Lu, K. Tieu, Y. Shibata, Dynamic interaction between grain boundary and stacking fault tetrahedron, *Scr. Mater.* 144 (2018) 78–83.
- [28] D. Farkas, A. Caro, Model interatomic potentials and lattice strain in a high-entropy alloy, *J. Mater. Res.* 33 (19) (2018) 3218–3225.
- [29] Y. Zhang, G.M. Stocks, K. Jin, C. Lu, H. Bei, B.C. Sales, L. Wang, L.K. Béland, R. E. Stoller, G.D. Samolyuk, Influence of chemical disorder on energy dissipation and defect evolution in concentrated solid solution alloys, *Nat. Commun.* 6 (1) (2015) 1–9.
- [30] Y. Li, R. Li, Q. Peng, Enhanced surface bombardment resistance of the CoNiCrFeMn high entropy alloy under extreme irradiation flux, *Nanotechnology* 31 (2) (2019), 025703.
- [31] Y. Liu, R. Li, Q. Peng, The preexisting edge dislocations as recombination center of point defects enhancing irradiation tolerance in CoCrCuFeNi high entropy alloy, *Materialia* 21 (2022), 101307.
- [32] X.-M. Bai, A.F. Voter, R.G. Hoagland, M. Nastasi, B.P. Uberuaga, Efficient annealing of radiation damage near grain boundaries via interstitial emission, *Science* 327 (5973) (2010) 1631–1634.
- [33] S. Plimpton, Fast parallel algorithms for short-range molecular dynamics, *J. Comput. Phys.* 117 (1) (1995) 1–19.
- [34] O. Deluigi, R. Pasianot, F. Valenciac, A. Caro, D. Farkas, E. Bringa, Simulations of primary damage in a High Entropy Alloy: Probing enhanced radiation resistance, *Acta Mater.* 213 (2021), 116951.

- [35] R. Stoller, A. Tamm, L. Béland, G. Samolyuk, G. Stocks, A. Caro, L. Slipchenko, Y. N. Ossetsky, A. Aabloo, M. Klintenberg, Impact of short-range forces on defect production from high-energy collisions, *J. Chem. Theory Comput.* 12 (6) (2016) 2871–2879.
- [36] J.F. Ziegler, J.P. Biersack, The stopping and range of ions in matter, Springer, Treatise on heavy-ion science, 1985, pp. 93–129.
- [37] H.J. Berendsen, J.v. Postma, W.F. Van Gunsteren, A. DiNola, J.R. Haak, Molecular dynamics with coupling to an external bath, *J. Chem. Phys.* 81 (8) (1984) 3684–3690.
- [38] A. Stukowski, Visualization and analysis of atomistic simulation data with OVITO—the Open Visualization Tool, *Model. Simul. Mater. Sci. Eng.* 18 (1) (2009), 015012.
- [39] X. Wang, N. Gao, W. Setyawan, B. Xu, W. Liu, Z. Wang, Effect of irradiation on mechanical properties of symmetrical grain boundaries investigated by atomic simulations, *J. Nucl. Mater.* 491 (2017) 154–161.
- [40] Z.H. Sun, J. Zhang, G.X. Xin, L. Xie, L.C. Yang, Q. Peng, Tensile mechanical properties of CoCrFeNiTiAl high entropy alloy via molecular dynamics simulations, *Intermetallics* 142 (2022), 107444.
- [41] L. Zhang, Y. Shibuta, C. Lu, X. Huang, Interaction between nano-voids and migrating grain boundary by molecular dynamics simulation, *Acta Mater.* 173 (2019) 206–224.
- [42] L. Zhang, C. Lu, K. Tieu, X. Zhao, L. Pei, The shear response of copper bicrystals with  $\Sigma 11$  symmetric and asymmetric tilt grain boundaries by molecular dynamics simulation, *Nanoscale* 7 (16) (2015) 7224–7233.
- [43] X. Li, W. Liu, Y. Xu, C.S. Liu, B.C. Pan, Y. Liang, Q.F. Fang, J.-L. Chen, G.N. Luo, G.-H. Lu, Z. Wang, Radiation resistance of nano-crystalline iron: coupling of the fundamental segregation process and the annihilation of interstitials and vacancies near the grain boundaries, *Acta Mater.* 109 (2016) 115–127.
- [44] Y.-K. Dou, H. Cao, X.-F. He, J. Gao, J.-L. Cao, W. Yang, Interaction mechanism of an edge dislocation with a void in Fe–Ni–Cr concentrated solid-solution alloy, *J. Alloy. Compd.* 857 (2021), 157556.